J. Fluid Mech. (2001), *vol.* 429, *pp.* 381–390. Printed in the United Kingdom

Viscous beads on vertical fibre

By I. L. KLIAKHANDLER[1], S. H. DAVIS[1] AND S. G. BANKOFF[2]

[1]Department of Engineering Sciences and Applied Mathematics, Northwestern University, Evanston, IL 60208, USA

[2]Department of Chemical Engineering, Northwestern University, Evanston, IL 60208, USA

(Received 3 October 2000 and in revised form 17 November 2000)

The dynamics of a thick layer of viscous liquid flowing down a thin vertical fibre is investigated. Three qualitatively different regimes of the interfacial patterns in the form of beads were observed experimentally. Two typical regimes at relatively small flow rate are described reasonably well by the creeping-flow model equation proposed here.

1. Introduction

Flows of liquid films on solid substrates have been the subject of interest because of the range of phenomena that they display (waves, rupture, contact lines, corners and cusps) and the importance of the applications in which they occur (photographic films and papers, depth probes, coating, mass/heat transfer). The ability to contour the free surface by 'designing' the proper flow gives one the potential of creating *in situ* objects of interest.

When the film is ostensibly planar, surface tension acts as a stabilizing mechanism that counterbalances the destabilization of Marangoni effects, or other externally imposed forces. See Lin (1983), Chang (1994) and Oron, Davis & Bankoff (1997) for reviews.

When the film is ostensibly cylindrical of radius a, surface tension acts to destabilize the interface by the usual Rayleigh (1878) mechanism. There is a tendency for the film to break up into axisymmetric droplets within the axial length scale $L > 2\pi a$; the infinitely long film cylinder is always unstable to breakup.

When there is axial flow in the film, the shear competes with capillarity; the breakup is restrained and instability is confined to much longer scales $L \gg 2\pi a$ (Xu & Davis 1985). This effect has been verified experimentally by Dijkstra & Steen (1991) using thermal forcing on a cylinder with a coaxial wire along the centreline. Experiments by Quéré (1990) and De Ryck & Quéré (1996) showed that mean shear in a film equilibrates growing disturbances. As a result, finite-amplitude interfacial waves were observed and breakup is avoided. The dynamics, structure and interaction of the drops were not investigated.

In the present work a thick viscous film of castor oil on a vertical wire is observed to become unstable and form beads, as shown in figure 1. The Reynolds number of the flow is very small, typically 10^{-2}.

It turns out that such creeping flows on thin fibre show a very rich dynamical behaviour, which apparently has not previously been considered experimentally or theoretically.

The theoretical description of the axisymmetrical interfacial dynamics has usually been in terms of the long-wavelength evolution equations using a technique of Benney

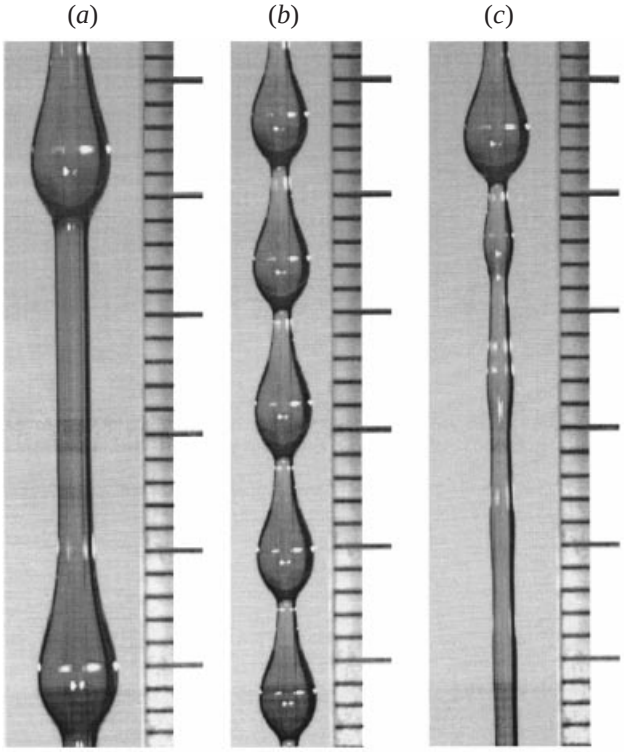

FIGURE 1. The typical droplet structures observed in experiments. Three wave profiles are measured at decreasing flow rates. The small marks on the ruler are 1 mm apart.

(1966). Such equations have been derived by Lin & Liu (1975) and by Atherton & Homsy (1976). Frenkel (1992) considered the limiting case of large cylinder radius (small film thickness) and derived a simple Benney-like equation for the film evolution. Kalliadasis & Chang (1994), Kerchman & Frenkel (1994) and Chang & Demekhin (1999) investigated the dynamics of Frenkel's (1992) equation, and compared the predictions with the experimental data of Quéré (1990).

The above papers deal with equations derived under the assumption of small film thicknesses. In our experiments, however, the film is at least twice as thick as the fibre radius. Therefore, the previously derived equations do not apply here. A model system will be posed that will describe Stokes flow, (constant) surface tension and gravity. When this system is solved, it predicts patterns close to those in figure 1.

2. Experimental results

The experimental part of the study was performed in the laboratory of Professor H.-C. Chang, Department of Chemical Engineering, University of Notre Dame. The help of Dr I. Veretennikov and Dr A. Indeikina in the construction of the experimental setup and taking of measurements was invaluable; we are deeply grateful to them.

The experimental setup is shown in figure 2(*a*). Castor oil (density $\rho = 0.961\,\mathrm{g\,cm^{-3}}$, kinematic viscosity $\nu = 4.4\,\mathrm{cm^2\,s^{-1}}$, surface tension $\gamma = 31\,\mathrm{g\,s^{-2}}$) coloured with SUDAN IV was placed in a large tank with a hole of about 1 mm diameter in its base. Nylon fishing line of radius 0.25 mm and length 2.5 m is passed downward through the hole and tethered to a weight that restrained the line to remain vertical. The flow

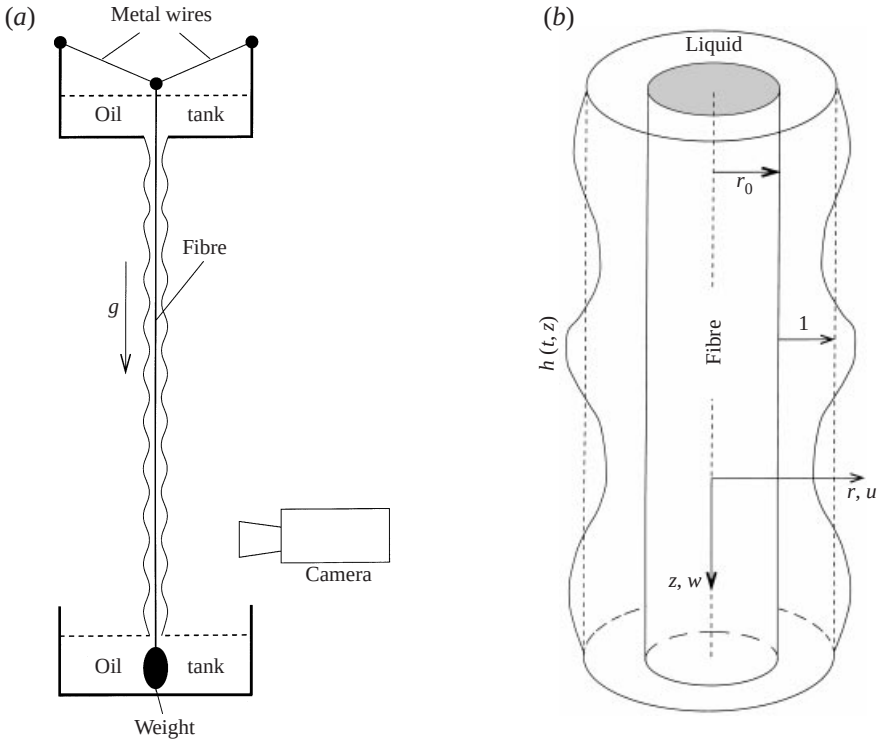

FIGURE 2. (*a*) The experimental setup. (*b*) The geometry of the film flow down a fibre.

	Flow rate Q, mm^3 s^{-1}	Mean film thickness h_0, mm	Distance between drops, cm	Velocity of drops, cm s^{-1}	Height of drops, mm	Minimal thickness of film, mm
Regime (a)	21.8	0.73	3.0	2.5	1.47	0.50
Regime (b)	11.5	0.62	0.62	0.54	1.02	0.20
Regime (c)	5.50	0.51	3.6	1.20	1.20	0.25

TABLE 1. The parameters of the experiments for the pictures on figure 1.

over the fibre was photographed using a high-resolution Kodak MegaPlus 1.6 digital camera at a position about 2 m below the orifice.

Figure 1 and table 1 show the results of the experimental runs at three different flow rates. Due to the difference in the optical density of the fibre and the oil, the fibre looks somewhat thicker than it actually is.

To find the equilibrium thickness h_0 of the film, one solves the equation and boundary conditions for unidirectional parallel flow on a fibre of radius $\bar{r}_0$:

$$\frac{g}{\nu} + r^{-1}(rW_r)_r = 0, \quad W(\bar{r}_0) = 0, \quad W'(h_0 + \bar{r}_0) = 0. \tag{2.1}$$

One finds that

$$W(r) = \frac{g}{4\nu}\left[2(h_0 + \bar{r}_0)^2 \log\frac{r}{\bar{r}_0} - r^2 + \bar{r}_0^2\right]. \tag{2.2}$$

Hence, the flow rate Q is the following function of the equilibrium thickness h_0:

$$Q(h_0) = 2\pi \int_{\bar{r}_0}^{\bar{r}_0+h_0} rW(r)\,\mathrm{d}r \tag{2.3}$$

$$= \frac{\pi g}{8\nu}\left[4(h_0+\bar{r}_0)^4 \ln\frac{h_0+\bar{r}_0}{\bar{r}_0} - h_0(3h_0^3 + 12h_0^2\bar{r}_0 + 14h_0\bar{r}_0^2 + 4\bar{r}_0^3)\right]. \tag{2.4}$$

For a given Q and $\bar{r}_0$, one obtains h_0.

As can be seen from figure 1, three distinct regimes of the flow were observed. The first regime is observed for relatively large flow rates, figure 1(*a*). In this case, the drops are large and move rapidly. The film between the drops is relatively thick and practically uniform. The average distance between the drops is relatively large, though the separation between the individual drops slightly varies. The large drops sometimes collide with each other in an irregular fashion; the process of collision is very fast.

In the second case, figure 1(*b*), the drop train is highly organized; the shape, speed and distance between the drops do not change over time. A detailed investigation of the digital image has shown the periodicity of the train. The speed and size of the drops are substantially smaller than those in regime (a). This regime was observed in a relatively small range of flow rates.

For very small flow rates, figure 1(*c*), the structure of the drops changes in an unexpected fashion. Namely, the drops become larger, they are substantially more separated in space, and the film in the space between the large drops is not uniform, but shows a periodic growth of disturbances. It is remarkable that the size and speed of the drops in regime (c) are larger than those in regime (b), though the flow rate in regime (c) is smaller. Since the distance between the drops is large, figure 1(*c*) shows only one large drop. Large drops collide with growing lobes ahead of them, consume them, and continue to move. During the collision, the large drops move faster. As a result, the instantaneous velocity of large drops changes periodically in time.

Overall, it is striking that this simple flow shows such rich interfacial dynamics, even though its Reynolds number is very small. Since the flow is axisymmetric, the diminishing of the flow rate from regime (a) to regime (c) results in relatively slow changes of all dimensionless parameters (see table 2 below).

Quéré (1990) has shown that when h_0 exceeds a critical thickness h_c, large capillary drops are formed. He obtained the relation $h_c = \alpha\bar{r}_0^3/H^2$, where the capillary length $H = (\sigma/\rho g)^{1/2}$. Kalliadasis & Chang (1994) constructed the lone stationary pulse and obtained the same law theoretically with numerical factor $\alpha = 1.68$. For the experiments of figure 1 $H = 1.8\,\mathrm{mm}$, and $h_c = 0.008\,\mathrm{mm} = 8\,\mu\mathrm{m}$. In experiments by Quéré (1990) with smaller surface tension and larger $\bar{r}_0$, it was found that $h_c = 17\,\mu\mathrm{m}$. The characteristic initial thickness h_0 of the film in the experiments in figure 1 is typically 0.5 mm. Therefore, in our experiments the film is about two orders of magnitude thicker than the critical thickness h_c. As a result, the observed interfacial waves are highly nonlinear.

3. Statement of the problem

Consider an axisymmetrical flow of liquid down a vertical fibre under gravity, figure 2(*b*). The surrounding gas is assumed to be weightless, quiescent, and inviscid with

	r_0	σ^{-1}	R
Regime (a)	0.34	6.20	0.020
Regime (b)	0.40	8.60	0.012
Regime (c)	0.50	12.5	0.007

TABLE 2. The dimensionless parameters for the experimental results on figure 1.

constant pressure p_0. The governing equations are

$$r^{-1}(ru)_r + w_z = 0, \tag{3.1a}$$

$$R(w_t + ww_z + uw_r) = 1 - p_z + r^{-1}(rw_r)_r + w_{zz}, \tag{3.1b}$$

$$R(u_t + wu_z + uu_r) = -p_r + [r^{-1}(ru)_r]_r + u_{zz}. \tag{3.1c}$$

Here r, z are the streamwise and radial coordinates, respectively, in units of the unperturbed film thickness h_0; u, w are the corresponding velocity components, referred to $\bar{W} = gh_0^2/\nu$, where g is the gravity acceleration; p is the pressure in units of $\rho g h_0$; t is the time referred to $h_0/\bar{W}$; $R = \bar{W}h_0/\nu = gh_0^3/\nu^2$ is the Reynolds number.

At the fibre surface, there is no penetration and no slip:

$$u(r_0) = w(r_0) = 0, \tag{3.2a}$$

where $r_0 = \bar{r}_0/h_0$.

At the free surface at $r = h(z,t)$ there is zero shear stress:

$$(1 - h_z^2)(w_r + u_z) + 2h_z(u_r - w_z) = 0. \tag{3.2b}$$

Normal stress is balanced by surface tension times curvature:

$$p - p_0 + 2[(w_r + u_z)h_z - u_r - h_z^2 w_z] + \sigma^{-1}\ 2H = 0. \tag{3.2c}$$

Here $\sigma = \rho g h_0^2/\gamma$ is the Bond number, where γ is the surface tension, and the mean curvature $2H$ is

$$2H = \frac{h_{zz}}{(1 + h_z^2)^{3/2}} - \frac{1}{(r_0 + h)(1 + h_z^2)^{1/2}}. \tag{3.3}$$

The kinematic boundary condition on the free surface is

$$h_t + wh_z - u = 0. \tag{3.4a}$$

Written in conservative form, (3.1*a*) and (3.4*a*) are

$$h_t + \frac{1}{r_0 + h}\frac{\partial}{\partial z}\int_{r_0}^{r_0+h} w\ r\,\mathrm{d}r = 0. \tag{3.4b}$$

Equations (3.1*a*)–(3.1*c*) together with boundary conditions (3.2*a*)–(3.2*c*) and (3.4*b*) constitute a free-boundary problem for $h(z,t)$.

In terms of dimensionless variables defined above the three regimes shown on figure 1 are specified by the parameters shown in table 2.

4. Linear stability problem

The linear stability analysis of the problem provides the first insight in the underlying interfacial dynamics. The numerical study of the pertinent Orr–Sommerfeld eigenvalue problem is the subject of the present section.

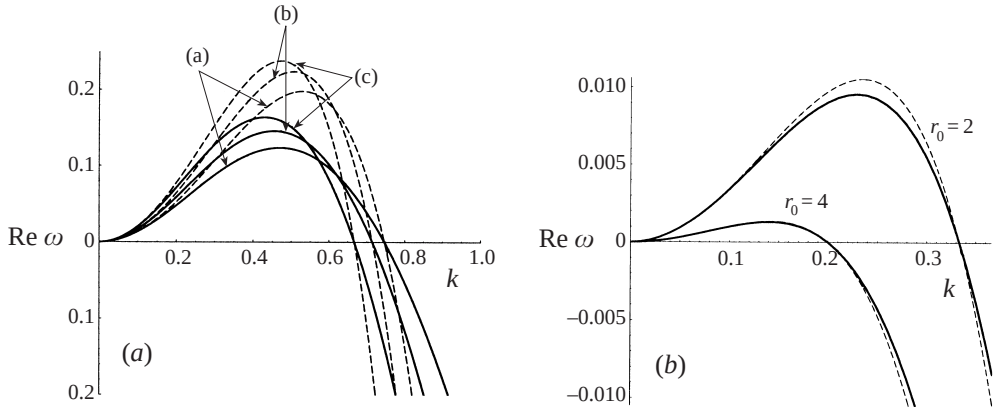

FIGURE 3. (*a*) Comparison of exact growth rates, Re(ω), the solid curve, versus that of the asymptotic theory, the dashed line. The flow parameters are given in table 1 and correspond to the conditions of experiment of figure 1 given in table 2. (*b*) Comparison of exact growth rate, Re(ω), solid line, versus the asymptotic theory, dashed line, for the thin films. Here $R = 0$ for both cases.

The steady-state unidirectional solution for (3.1*a*)–(3.1*c*) is

$$h = 1, \quad p = p_0, \quad W(r) = \frac{1}{4}\left[2(1+r_0)^2 \log\frac{r}{r_0} - r^2 + r_0^2\right]. \tag{4.1}$$

The linear stability analysis of flow (4.1) includes the following manipulations: linearization (3.1*a*)–(3.1*c*), (3.2*a*)–(3.2*c*) and (3.4*b*) near (4.1), introduction of the stream function $\psi(z, r, t)$ for the disturbed flow, and use of the normal mode decomposition,

$$\psi(z, r, t) = \phi(r)\mathrm{e}^{\mathrm{i}kz+\omega t}, \quad h = 1 + \eta, \quad \eta = a\mathrm{e}^{\mathrm{i}kz+\omega t}. \tag{4.2}$$

The result is the Orr–Sommerfeld eigenvalue problem for $\phi(r)$ in cylindrical geometry (Lin & Liu 1975; Atherton & Homsy 1976; Homsy & Geyling 1977). We concentrate on a temporal formulation of the stability problem, with real k and complex ω.

A shooting method combined with the Newton–Raphson algorithm has been used to solve the boundary-value problem. The procedure involves two main steps: a guess of initial values for integration, and iterations to reach the solution. As an initial guess, cubic extrapolation of the initial values of solutions for smaller k has been chosen. For very few initial points, the long-wavelength asymptotic solution was used as an initial guess. The Jacobian matrix was evaluated by second-order central differencing. The Runge–Kutta fourth-order method was used for the integration.

The results of the computations for cases (a), (b), and (c) are shown on figure 3(*a*). In these computations, the Reynolds number is taken to be zero. It was checked that the full dispersion relations (with very small but finite Reynolds numbers R and not shown here) are very close to those with zero Reynolds number. The dispersion relations for the thin film are shown in figure 3(*b*). We shall use the curves obtained to test the evolution equation posed in the next section.

5. Nonlinear evolution equation

There are several possibilities for the derivation of simplified evolution equations that describe the interfacial dynamics in the terms of surface shape. First, the long-wavelength expansions by Benney (1966) can be adopted. In the application of the

approach to the planar film flows down an incline, the surface tension is assumed to be large. As a result, the waves are long, surface slopes are small, and surface-tension effects are retained in the leading-order approximation.

For the film flow down the cylinder the situation is different. Here the surface tension affects both streamwise and radial disturbances, and even if surface tension is large, this does not guarantee that the waves will be long. As a result, the typical size of the disturbances is affected by the shear, and the surface slopes might be of order unity. As may be seen from the experimental pictures (figure 1), though the waves are quite long, wave gradients may be of order unity. This means that formal application of Benney expansions will require several successive iterations. This approach does not lead to a simple model.

An approximation of boundary-layer type might also be contemplated as an alternative (see Chang 1994). Such an approach does not lead to a simple model, even for creeping flow.

As a result, we take the following view. We consider the equations of creeping flow. We assume that in the normal-stress condition the pressure jump dominates the viscous forces: a small capillary number approximation. As a result,

$$p = p_0 + \sigma^{-1}\left[\frac{h_{zz}}{(1+h_z^2)^{3/2}} - \frac{1}{(r_0+h)(1+h_z^2)^{1/2}}\right], \tag{5.1}$$

where p_0 is the atmospheric pressure. Note that we include the full curvature term without approximation as was proposed in other contexts by Rosenau, Oron & Hyman (1992). This is motivated by the large amplitude of the waves, and relatively large interface gradients. We assume that the velocity profile is slowly varying, and neglect the w_{zz} term in the streamwise momentum equation (3.1*b*), and all terms of order $\partial/\partial z$ in boundary condition (3.2*b*). The velocity profile is therefore described by the following system:

$$1 - p_z + r^{-1}(rw_r)_r = 0, \quad w(r_0) = 0, \quad w_r(r_0+h) = 0. \tag{5.2}$$

Solving (5.2) and substituting the result in kinematic boundary condition (3.4*b*) results in the following equation:

$$h_t + \frac{1}{r_0+h}\left[Q(h) + \sigma^{-1}Q(h)\left(\frac{h_{zz}}{(1+h_z^2)^{3/2}} - \frac{1}{(r_0+h)(1+h_z^2)^{1/2}}\right)_z\right]_z = 0, \tag{5.3}$$

where

$$Q = \frac{1}{16}\left[4(h+r_0)^4 \log\frac{h+r_0}{r_0} - h(3h^3 + 12h^2r_0 + 14hr_0^2 + 4r_0^3)\right]. \tag{5.4}$$

Equation (5.3) has not been derived asymptotically; it is a *model* equation. We shall assess the applicability of the model from a comparison of its linear stability with the full linear stability problem, and from a direct comparison of the numerical simulation of (5.3) with experiment.

In the context of the film flow on the fibre, equation (5.3) is asymptotically valid only for small film thicknesses (Frenkel 1992). We, however, shall use equation (5.3) to investigate the flow of a thick film.

Linear analysis of (5.3) gives

$$\omega = \sigma^{-1}A\left[\frac{k^2}{(1+r_0)^2} - k^4\right], \tag{5.5}$$

	Distance between drops, cm	Speed of drops, cm s^{-1}	Height of drops, mm	Minimal thickness of film, mm
Experiment	0.62	0.54	1.020	0.20
Simulations	0.72	0.80	1.025	0.19

TABLE 3. Comparison of experimental results with simulations.

where

$$A = \frac{1}{16(1+r_0)}\left[-3-12r_0-14r_0^2-4r_0^3+4(1+r_0)^4\log\frac{1+r_0}{r_0}\right]. \tag{5.6}$$

Comparison of dispersion relations (5.5) with the exact dispersion relations is given in figure 3. It is seen that the asymptotic dispersion relation (5.5) gives excellent approximations of the exact relation when the film is thin, figure 3(*b*). The most unstable mode of approximate model (5.5) coincides with that of Rayleigh (1878) and the cut-off wavenumbers for the approximate and exact dispersion relations coincide. The agreement between the two dispersion relations for the thick film, figure 3(*a*), is qualitatively good and demonstrates that (5.3) is a reasonable model.

6. Results of numerical simulations

Equation (5.3) subject to periodic boundary conditions was simulated by a standard pseudospectral technique. The Runge–Kutta fourth-order scheme was used for the time advance. The spatial discretization was such that the typical wavelength $\lambda = 2\pi/k_m$ of the most unstable wavenumber k_m was covered by at least 12 points to ensure fair resolution of the computed solutions. Conservation of the flow invariant $h_0 r_0 + h_0^2/2$ was carefully monitored. The typical time step was 10^{-3}. Tests with smaller time steps gave indistinguishable results. Random small-amplitude fields or periodic functions were used as initial conditions. Typically, the simulations were conducted on long spatial intervals (up to 40λ), though only part of the intervals are presented on the figures to make the wavy structures clear.

The main results of the simulations are as follows. For the small-amplitude random initial data and data for regime (b) (table 2), model (5.3) gives typical periodic structures shown on figure 4(*a*). The amplitude, length and form of the drops are very close to those of figure 1(*b*). A comparison of the experiment with simulation in this case is given in table 3.

For regime (c), the small-amplitude initial data give similar periodic structures. However, for long-scale periodic initial data with noise, the structure of the waves is close to those observed in figure 4(*a*). In the latter case, the amplitude of the drops is 1.2 mm, as in the experiment. The form of the bead pattern is close to that observed in regime (c), though the distance between the drops is about half that in the experiment. It is remarkable that for the small flow rate, regime (c), the periodic flow in experiment extends up to the source and is similar to the periodic initial conditions: the liquid leaks down to the fibre periodically in the form of drops. The interaction between the large drops and small varicosities is shown in figure 4(*b*). The large drops collide with small drops and subsume them; the whole process is periodic in time. The dynamics in figure 4(*b*) is close to the experimentally observed structures on figure 1(*c*). Regime (a) however was not reproduced by model (5.3). The

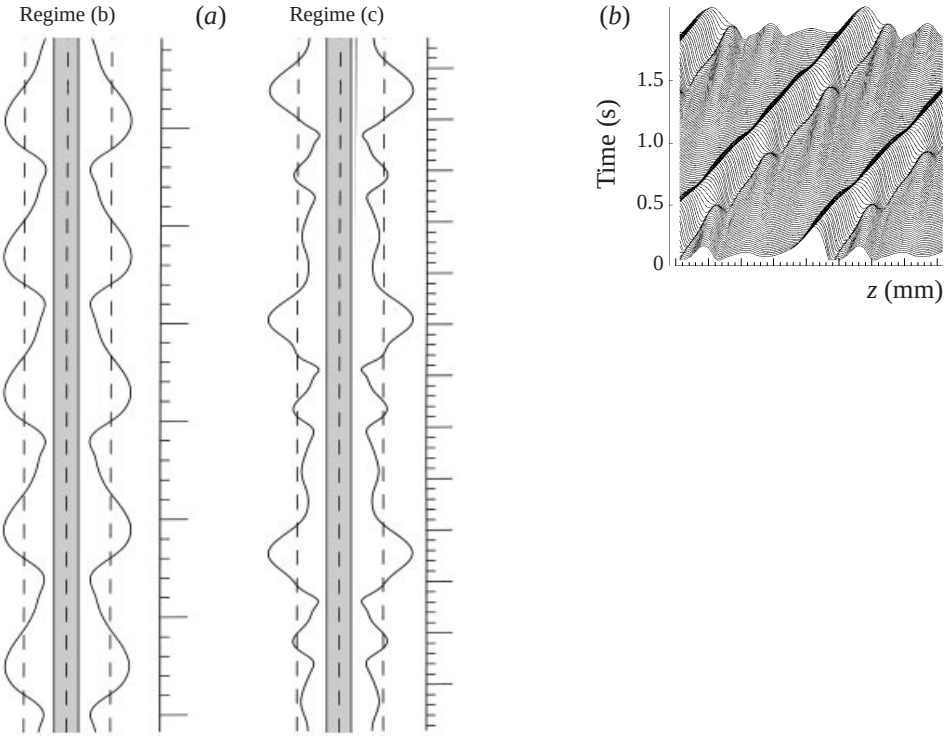

FIGURE 4. Solution of model (5.3): (*a*) profiles for regimes (b) and (c); (*b*) spatio-temporal dynamics for regime (c).

main feature of the regime, the virtually uniform interface between large drops, is not captured.

Note that two different scenarios have been proposed to explain the formation of the pulses with a smooth interface between them in thin weakly nonlinear films. Chang, Demekhin & Kalaidin (1998) considered a drainage mechanism, leading to the generation of the smooth film between the beads on the basis of a generalized KS equation including dispersion (Kawahara equation). The distance between the beads separated by smooth film might be three times longer than the most unstable wave. The Kawahara equation is derived for thin planar films near the onset the instability and is weakly nonlinear, so that it does not apply to the present situation of thick strongly nonlinear axisymmetric films and beads. However, the analysis done by Chang *et al.*(1998) does reveal qualitative features similar to those observed in all three regimes.

On the other hand, Kalliadasis & Chang (1994), Kerchman & Frenkel (1994), Kerchman (1995), Chang & Demekhin (1999) considered the strongly nonlinear model derived by Frenkel (1992) for axisymmetric thin films. Kerchman & Frenkel (1994) and Kerchman (1995) found that the model produces large pulses with a flat interface between them. Kalliadasis & Chang (1994) constructed a solitary pulse solution and Chang & Demekhin (1999) found the asymptotic blow-up solutions in Frenkel's equation. The tendency of the solutions of Frenkel's equation to blow-up was interpreted as a predisposition of the system to the drop formation.

The dynamics of thick films observed in regime (a) is strongly nonlinear and appears in cylindrical geometry. Therefore, it is not clear which scenarios described

above and discovered in weakly nonlinear models of planar thin films are responsible for the formation of large beads (pulses) in regime (a).

7. Conclusion

This paper investigates the formation of viscous beads on a thin fibre experimentally and theoretically. Three different regimes of bead dynamics are observed for creeping flows as shown in figure 1. A simple model equation based on consideration of the Stokes flow is proposed and results of a numerical simulation are in a good agreement with two of three modes seen in experiment.

This work was supported by the Engineering Research Program of the Office of Basic Energy Sciences at the Department of Energy.

REFERENCES

Atherton, R. W. & Homsy, G. M. 1976 On the derivation of evolution equations for interfacial waves. *Chem. Engng Commun.* **2**, 57–77.

Benney, D. J. 1966 Long waves on liquid films. *J. Math. Phys.* **45**, 150–155.

Chang, H.-C. 1994 Wave evolution on a falling film. *Ann. Rev. Fluid Mech.* **26**, 103–136.

Chang, H.-C. & Demekhin, E. A. 1999 Mechanism for drop formation on a coated vertical fibre. *J. Fluid Mech.* **380**, 233–255.

Chang, H.-C., Demekhin, E. A. & Kalaidin, E. 1998 Generation and suppression of radiation of solitary pulses. *SIAM J. Appl. Maths* **58**, 1246–1277.

De Ryck, A. & Quéré, D. 1996 Inertial coating of a fibre. *J. Fluid Mech.* **311**, 219–237.

Dijkstra, H. A. & Steen, P. H. 1991 Thermocapillary stabilization of the capillary breakup of an annular film of liquid. *J. Fluid Mech.* **229**, 205–228.

Frenkel, A. L. 1992 Nonlinear theory of strongly undulating thin films flowing down vertical cylinders. *Europhys. Lett.* **18**, 583–588.

Homsy, G. M. & Geyling, F. T. 1977 A note on instabilities in rapid coating of cylinders. *AIChE J.* **23**, 587–590.

Kalliadasis, S. & Chang, H.-C. 1994 Drop formation during coating of vertical fibres. *J. Fluid Mech.* **261**, 135–168.

Kerchman, V. I. 1995 Strongly nonlinear interfacial dynamics in core-annular flows. *J. Fluid Mech.* **290**, 131–166.

Kerchman, V. I. & Frenkel, A. L. 1994 Interactions of coherent structures in a film flow: simulations of a highly nonlinear evolution equation. *Theor. Comput. Fluid Dyn.* **6**, 235–254.

Lin, S. P. 1983 Film waves. In *Waves on Fluid Interfaces* (ed. R. P. Meyer), pp. 261–289. Academic.

Lin, S. P. & Liu, W. C. 1975 Instability of film coating of wires and tubes. *AIChE J.* **21**, 775–782.

Oron A., Davis, S. H. & Bankoff, S. G. 1997 Long-scale evolution of thin liquid films. *Rev. Mod. Phys.* **69**, 931–980.

Quéré, D. 1990 Thin films flowing on vertical fibers. *Europhys. Lett.* **13**, 721–726.

Rayleigh, Lord 1878 On the instability of jets. *Proc. Lond. Math. Soc.* **10**, 4–13.

Rosenau, P., Oron, A. & Hyman, J. M. 1992 Bounded and unbounded patterns of the Benney equation. *Phys. Fluids A* **4**, 1102–1104.

Xu, J. J. & Davis, S. H. 1985 Instability of capillary jets with thermocapilarity. *J. Fluid Mech.* **161**, 1–25.